Radiation Detection Technology and Methods (2019) 3:4
https://doi.org/10.1007/s41605-018-0047-1

ORIGINAL PAPER

Influence of energy bandwidth of pink beam on small angle X-ray scattering

Shanfeng Wang[1,2] · Yaxiang Liang[1] · Bingjie Wang[1,3] · Weiwei Dong[1,2] · Lingfei Hu[1] · Qun Ouyang[1] · Peng Liu[1]

Received: 27 February 2018 / Revised: 22 March 2018 / Accepted: 27 March 2018 / Published online: 22 October 2018

Abstract

Background Compared with the traditional monochromatic synchrotron radiation beam, a pink beam is a quasi-monochromatic beam which can be obtained by screening a harmonic of the undulator. The energy bandwidth ($\Delta E/E$) of a pink beam is about 10^{-2}. Despite the intensity gain from the quasi-monochromatic beam, the decrease in the energy resolution will lead the collected data to be smeared.

Purpose To study the influence of the energy bandwidth on the small angle X-ray scattering (SAXS) by experiments and verify the feasibility of SAXS with a pink beam.

Method Firstly, the influence of different energy bandwidths on SAXS has been studied by simulation and experiment. Then, TEM tests have been performed and compared with the experimental results.

Result It has been shown that the scattering curves deviate slightly from the traditional monochromatic ones. This deviation does not influence the data processing for the maximum deviation of the results is just less than 2%. In return, the gain in the intensity (one to two orders of magnitude) makes the pink beam very important for the time-resolved SAXS. Further, the results of TEM and SAXS have shown an excellent agreement.

Conclusion This work proves that the pink beam could be used for SAXS directly without a desmearing procedure. Benefiting from the increase in the beam intensity, the exposure time can be greatly shortened, thus enhancing the utilization efficiency of the synchrotron radiation.

Keywords Small angle X-ray scattering (SAXS) · Pink beam · Adjustable energy bandwidth · Smeared effect

Introduction

Small angle X-ray scattering (SAXS) is widely used for nanoscale structural research (1–1000 nm). This method mainly studies structures (particle shape, particle size, distribution, etc.) of 'particles' dispersed in homogeneous medium. Since the first use of SAXS to study the non-uniform structure information in alloy, the theory of SAXS has been developed and improved rapidly [1–5].

✉ Peng Liu
liup@ihep.ac.cn

[1] Beijing Synchrotron Radiation Facility, Institute of High Energy Physics, Chinese Academy of Sciences, Beijing 100049, People's Republic of China

[2] University of Chinese Academy of Sciences, Beijing 100049, People's Republic of China

[3] Zhengzhou University, Zhengzhou, Henan 450001, People's Republic of China

The synchrotron radiation beamline used to collect SAXS data is usually monochromatic with the energy resolution ($\Delta E/E$) of about 10^{-4}. For the weak signal samples, the decrease in the flux from the source when using traditional monochromatic beam will lead to the degradation of the collected data, sometimes even to the failure of the experiment. On the other hand, the intrinsic spectrum of an undulator is 'pink,' i.e., quasi-monochromatic with an energy bandwidth from 1 to 10% [6,7]. That means the intensity of a pink beam could be hundreds of times higher than that of a monochromic beam, which will enhance the signal of SAXS significantly and make the pink beam very promising for time-resolved experiments. Now, a few beamlines can collect SAXS data with the pink beam for the experiments requiring a very high beam intensity [8–12].

Although the pink beam has the advantage of high intensity, the reduction in the energy resolution may affect the collected data. In principle, SAXS deals with the relation

between the scattering intensity $I(q)$ and the scattering vector q, where $q = (4\pi \sin\theta)/\lambda$. Since SAXS is mainly concentrated in a small angle near the direct beam, the effect of the energy divergence, in other words the uncertainty of the scattering vector q, on bio-macromolecule SAXS data has been analyzed theoretically [13–16]. The theoretical results have shown that the energy divergence effect significantly depends on the geometry of the body and spherical particles are more susceptible [13]. Therefore, it is worthwhile to study the same effect on inorganic particles system and verify the results by experiment. With these verifications, SAXS with a pink beam could be proposed for improving the utilization efficiency of the synchrotron radiation.

This paper aims to reveal the influence of the energy bandwidth on SAXS and verify the feasibility of SAXS with a pink beam. Firstly, the influence of the energy bandwidth on SAXS was simulated by the ray-tracing software McXtrace. Secondly, a SAXS system with an adjustable energy bandwidth was adapted from 1W2B beamline's existing equipment at Beijing Synchrotron Radiation Facility (BSRF). Thirdly, a series of SAXS experiments were carried out with different energy bandwidths. Finally, transmission electron microscopy (TEM) tests were performed and compared with SAXS results.

Simulation

Simulation experiment

McXtrace is general Monte Carlo ray-tracing software for simulating X-ray beamlines and experiments, distributed under the open source license of GPL [17]. The software now works well and spans a range of X-ray experimental techniques, such as small angle X-ray scattering, absorption tomography, powder diffraction, single-crystal diffraction and pump-and-probe experiments. In this paper, McXtrace is used to carry out SAXS experiments simulation, and the influence of the energy bandwidth on SAXS is analyzed theoretically.

In the simulation experiment, the source with a flat spectrum was used. The energy bandwidth of the source can be adjusted according to the experimental requirement. The system used double slits to collimate the X-ray beam, whose sizes were the same as that of the experiment station. The sample was placed 100 mm downstream from the second slit, and the spherical particles with a radius R of 70 Å were selected. The detector was placed 1220 mm downstream from the sample, and the pixel sizes were the same as that of the detector used in the experiment: $172 \times 172\,\mu m^2$. The simulated SAXS experiments conducted 13 different energy bandwidths, from monochromatic gradually increased to 7%.

Simulation result

The scattering patterns were transformed into 1D scattering curves by fit2d, as shown in Fig. 1a. It shows that the dispersion of the energy makes the peak of SAXS curves to be dampened and the minimal value to be increased. The deviations of the scattering intensity between that collected with the pink beam and the monochromatic beam are shown in Fig. 1b, which is defined as deviation $= \left(I_{\text{poly}} - I_{\text{mono}}\right)/I_{\text{mono}}$. It shows that the deviation caused by the energy bandwidth just occurs near the sharp trough and is slight for the smooth range.

The relationship between the distance distribution function $P(r)$ and the scattering intensity is [18,19],

$$P(r) = \frac{1}{2\pi^2}\int_0^\infty qrI(q)\sin(qr)\,\mathrm{d}q, \tag{1}$$

where $P(r)$ is a function describing the structure information of the sample in real space. Some structure information of the sample can be obtained by $P(r)$ directly, for example the maximum size (Dmax) and the shape of the sample particles [20]. As shown in Fig. 1c, the corresponding distance distribution functions were obtained by the software GNOM [18]. Figure 1c shows that $P(r)$ will exhibit a slight deviation past the peak value as the energy bandwidth changes, but the shape of $P(r)$ almost remains the same, indicating that the shape of the particles is still spherical.

The Rg [21] and Dmax of particles are shown in Fig. 2a, b, respectively. The curves in Fig. 2a show that the radius of the gyration just changes a little with the increase in the energy bandwidth, and the difference is less than 1.5% relative to the ideal size. The Dmax does not change until the energy bandwidth increases to 7%.

SASfit was used to fit the SAXS curves of the simulation experiment; the results are shown in Fig. 3a, and the calculated particle sizes are shown in Fig. 3b. Figure 3a shows that the fitting curves can overlap well with the simulated ones except for the region near the sharp trough. Figure 3b shows that particle sizes obtained from different energy bandwidths are in high consistency and the maximum deviation is less than 0.1%.

Experiment

SAXS system with adjustable energy bandwidth

To collect SAXS data with different energy bandwidths, an experimental system with an adjustable energy bandwidth has been designed. The system is adapted from 1W2B beamline's existing equipment at BSRF. The control program of the monochromator is improved to make the double-

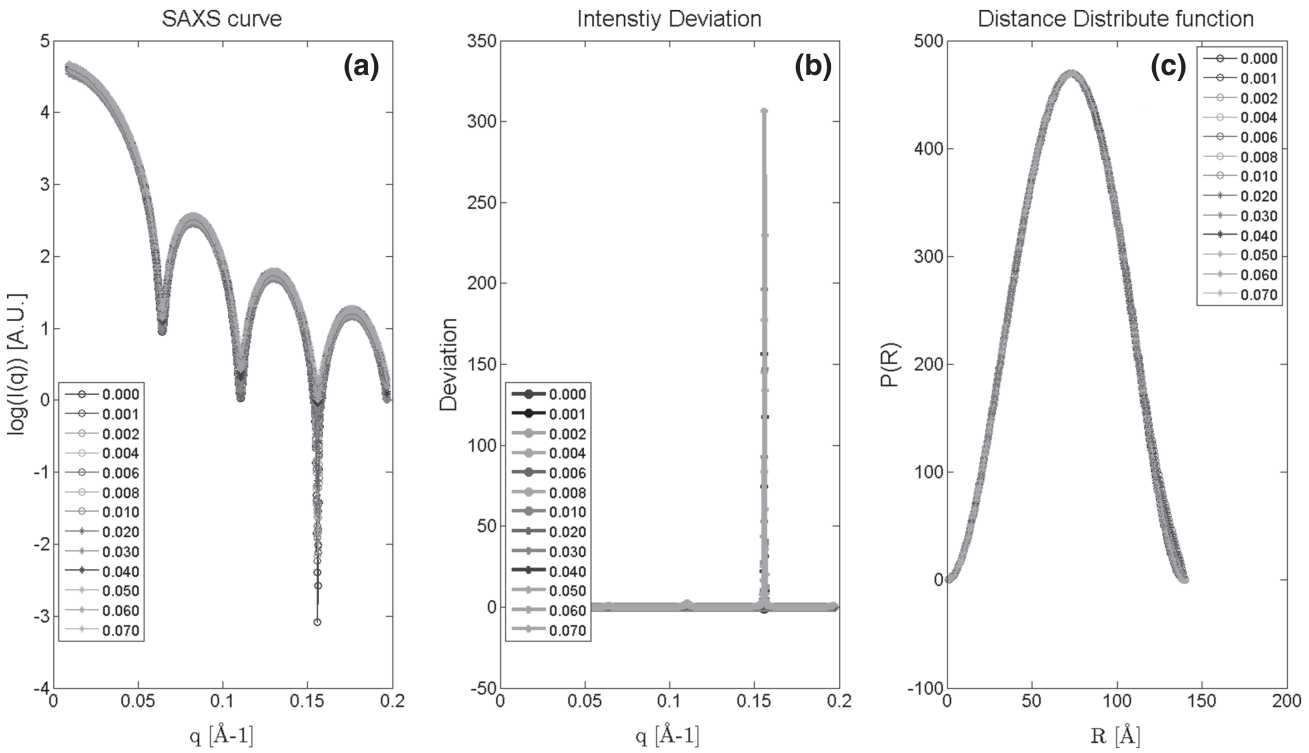

Fig. 1 Scattering curves of the simulation and the results of the SAXS. **a** The SAXS curves from simulation with different energy bandwidths. **b** The deviation of the scattering intensity between that collected with pink beams and monochromatic beam. **c** The distance distribution functions for different energy bandwidths

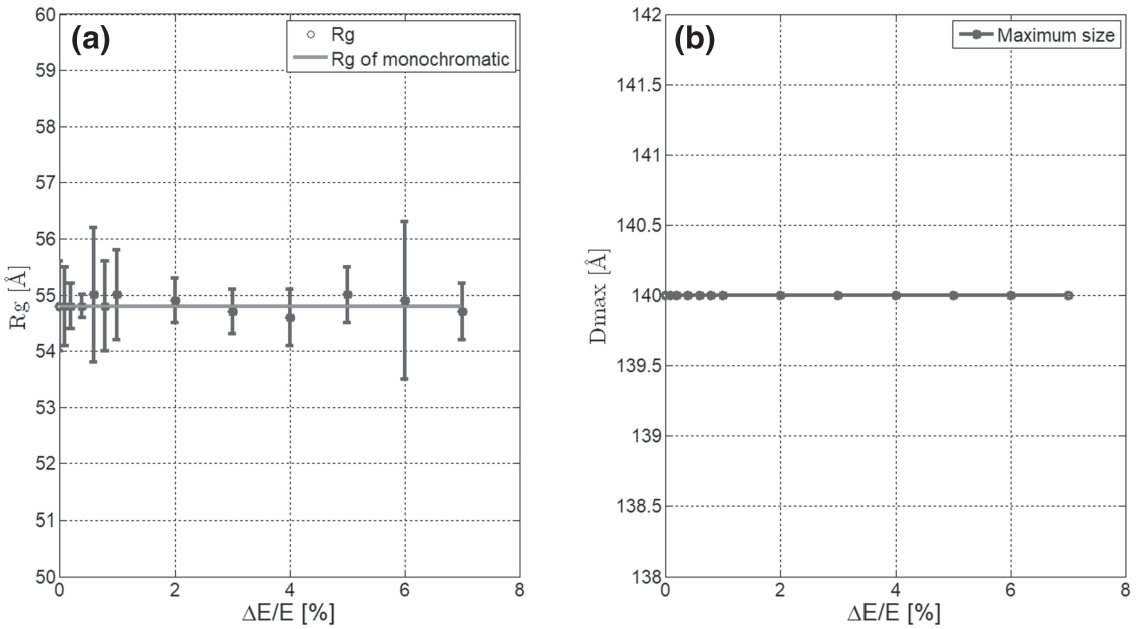

Fig. 2 Results of the simulation experiments. **a** The Rg curve with error bar calculated by Guinier law and the ideal size (red line). **b** The maximum size fitted from the distance distribution function (color figure online)

crystal monochromator reciprocate within a given energy bandwidth. The energy resolution of the double-crystal monochromator is about 10^{-4}, and the reciprocating step length of the double-crystal monochromator is 1 eV. To con-

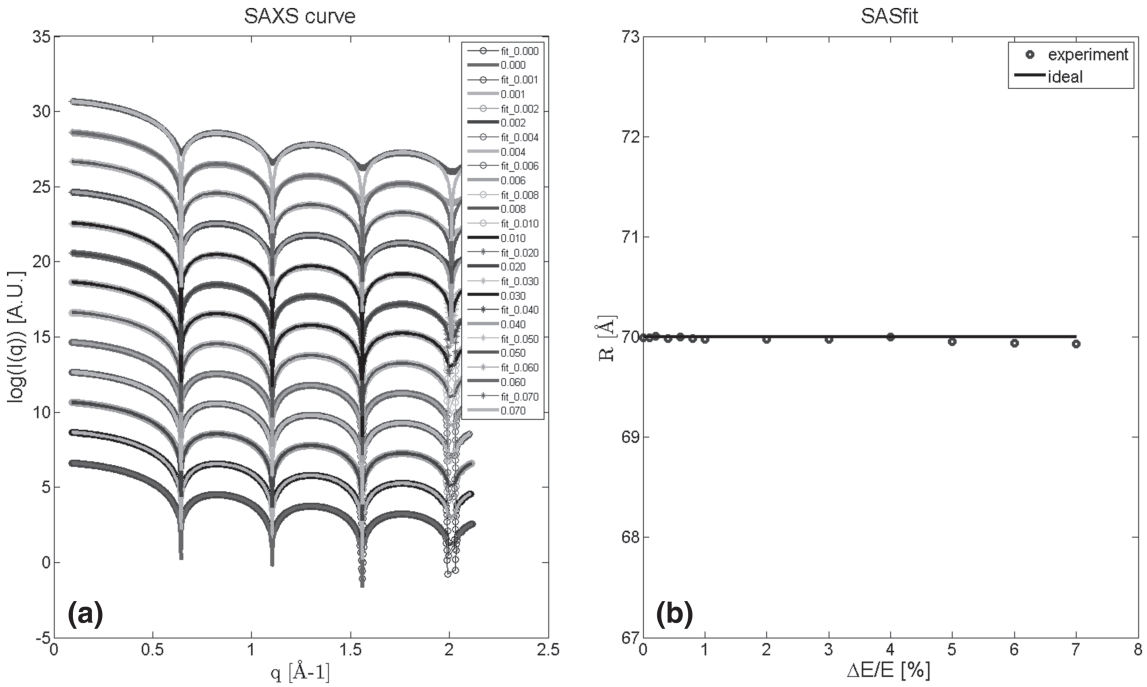

Fig. 3 **a** The fitted curves by SASfit. Offsets were added to make the curves intuitive. **b** The particle size fitted by SASfit. The black curve is the size used for simulation

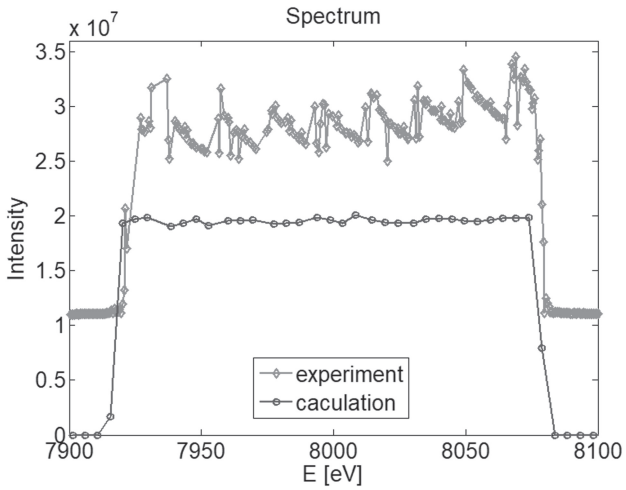

Fig. 4 The spectrum of the incident beam with a bandwidth of $\Delta E/E = 2\%$ at 8 keV. Intensity of experiment has an offset of 1.1×10^7

firm the reliability of the system, the energy spectrum is measured by a crystal and the result is shown with a red curve in Fig. 4. The spectrum obtained by the simulation is represented by a blue curve in Fig. 4. The results show that the energy bandwidth obtained by the system is consistent with the settings and the simulated spectral.

Sample preparation

The nanoparticle samples were synthesized at National Center for Nanoscience and Technology (NCNST) by Prof. Wang Zhen-gang et al. The resulting batch of 1 ml sample was used to fill 20 sample cells for collecting SAXS data with different energy bandwidths. The buffer used to get background signal was pure water filled in the same sample cells with a thickness of 1 mm.

Small angle X-ray scattering experiment

The experiments were completed in beamline 1W2B at BSRF. The experimental station is equipped with Xenocs' SAXS system with a Pilatus3R 1M detector. The sample-to-detector distance is 1215 mm, and the center energy of the X-ray is 8 keV ($\lambda = 1.5498$ Å). Sixteen sets of SAXS data with different energy bandwidths were collected with the system described above. For the pink beam the expose time equals to the period of the monochromator, which means the expose time for every energy point is equal. The energy bandwidth and the corresponding exposure time are shown in Table 1. As the energy bandwidth increases to 6%, the count of detector near the direct beam approaches saturation, and so the energy bandwidth for SAXS data acquisition ends up to 6%.

The experimental conditions must be consistent except the bandwidth and meet the basic needs of the experiment. For example: (1) The scattering vector range covers the basic requirement of $0.01 \leq q\,[\text{Å}^{-1}] \leq 0.21$; (2) for different energy bandwidths, the scattered signal of buffer sealed by tape must be collected; and (3) the direct beam intensity of

Table 1 Energy bandwidth and corresponding expose time

Bandwidth (%)	0.01	0.2	0.4	0.6	0.8	1	1.5	2
Expose time (s)	20	13	26	39	52	65	98	130
Bandwidth (%)	2.5	3	3.5	4	4.5	5	5.5	6
Expose time (s)	163	195	228	260	292	326	355	401

the sample and buffer must be recorded by a diode detector on the beam stop.

Data preprocessing

The collected SAXS data are 2D patterns, and the following steps are required for specific processing:

(a) Convert 2D scattering patterns into 1D curves and unify the scattering vector units into $[q] = \text{Å}^{-1}$.
(b) The scattering vector is controlled in a specific range ($0.01 \leq q(\text{Å}^{-1}) \leq 0.21$), which is sufficient to analyze the sample information.
(c) Background signal must be subtracted for different energy bandwidths, especially the signal of the solvent and tape.
(d) The exposure time of the traditional monochromatic beam is not equal to that of the pink beam, which should be adjusted before the data analysis.
(e) The intensities for different energy bandwidths should be normalized before analyzing the difference in scattering curves and structure information of the sample.

Sample characterization by TEM

The size and shape of samples were measured by TEM using a JEM-2100 microscope, and the operating voltage is 200 kV. Samples for TEM were prepared by placing a drop of about 6 times diluted nanoparticles solution on an amorphous carbon-coated copper grid and then placing it in the oven for 2 min to accelerate the drying of the solvent. The size and the distribution of samples are obtained by measuring the maximum size of all samples in the same direction (horizontal direction). Then, the measured sample size is fitted with the lognormal function, and the mean size (Rmean) and the standard deviation (σ) were derived from the fitting [22].

Results and discussion

Experimental results

The collected scattering curves are shown in Fig. 5a. Scattering curves display characteristic peaks at $q = 0.0836\,\text{Å}^{-1}$ and $q = 0.132\,\text{Å}^{-1}$ for different energy bandwidths and the characteristic peaks of the scattering curves do not change with the energy bandwidth, which is a typical indication of particles with a very narrow size distribution [23].

The relationships of Rg and $I(0)$ with energy bandwidth are shown in Fig. 5b, c, respectively. Figure 5b shows that the Rg almost keeps constant, and the fluctuation range is less than 0.2%. Figure 5c shows that the flux of the incident beam increases almost linearly with the bandwidth, which means the utilization efficiency of the synchrotron radiation source is proportional to the energy bandwidth.

The $P(r)$ obtained by Eq. (1) is shown in Fig. 6a, and the maximum size of the particles is shown in Fig. 6b. The function $P(r)$ is almost symmetric with a little deviation from each other, which means that the shapes derived from the patterns are spherical and just have a little difference for different energy bandwidths. Noticeable differences of $P(r)$ appear only in regions of higher values of radius. This difference results in an impact on maximum size of particle (Dmax), and the Dmax is shown in Fig. 6b as a blue circle. Figure 6b shows that the maximum size changes within a small range, approximately 2% relative to that obtained with the traditional monochromatic beam.

The intensity of the incident beam is normalized to compare the deviations, as shown in Fig. 7a. The deviations between scattering intensities collected with the pink beam and the traditional monochromatic beam are shown in Fig. 7b. Like the simulation, the deviation just occurs near the sharp trough. For the smooth range, it is less than 3%, which is within tolerance [24,25].

We found that the scattering curves are reproduced well using the analytical form factor of a sphere, $I_\text{q}(q, R, \Delta\eta)$, with a lognormal number-weighted size distribution of the radii, $f(R, N, \sigma, \mu)$, as [26–28]

$$I(q) = \int_0^\infty f(R, N, \sigma, \mu)\, I_\text{q}(q, R, \Delta\eta)\, \text{d}R, \tag{2}$$

where $f(R, N, \sigma, \mu)$ and $I_\text{q}(q, R, \Delta\eta)$ stand for the lognormal size distribution and the scattering of a single sphere, which are given by

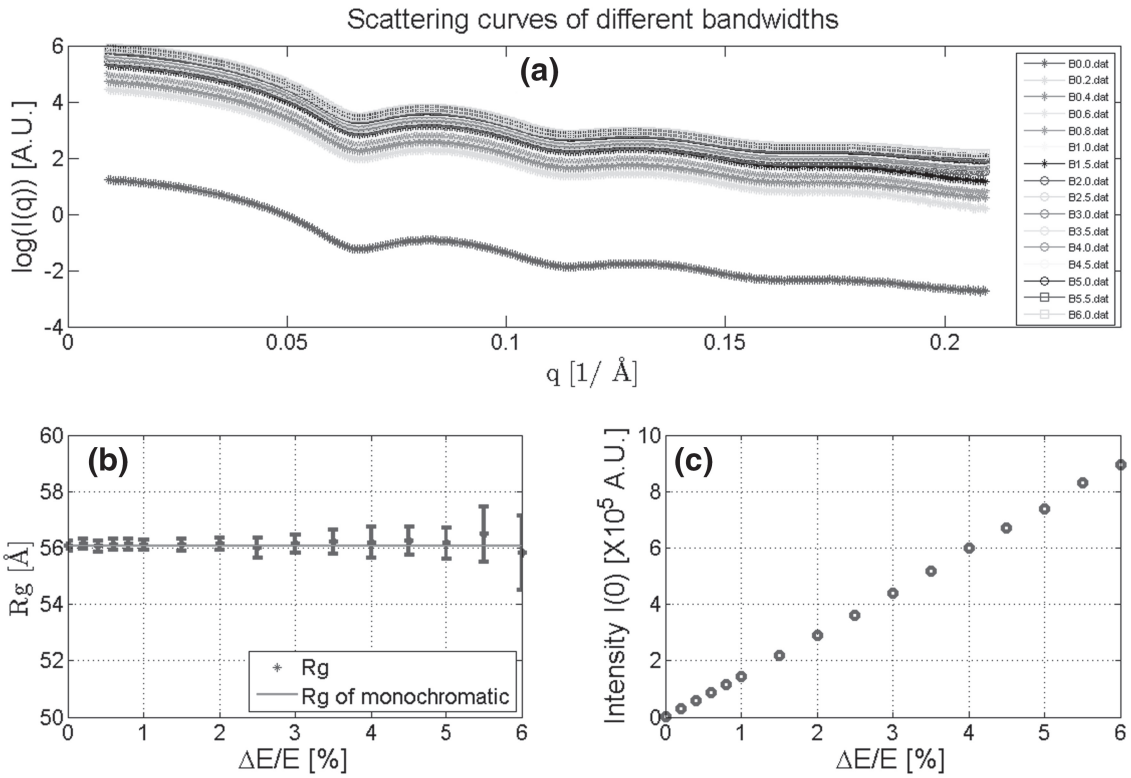

Fig. 5 The time-normalized SAXS curves for different bandwidths in (**a**). The first B 0.0 represents the double-crystal monochromic, the following for bandwidth 0.2, 0.4, 0.6%, and so on. The radius of gyration (**b**) and the forward scattering intensity (**c**) are calculated from the curves in (**a**)

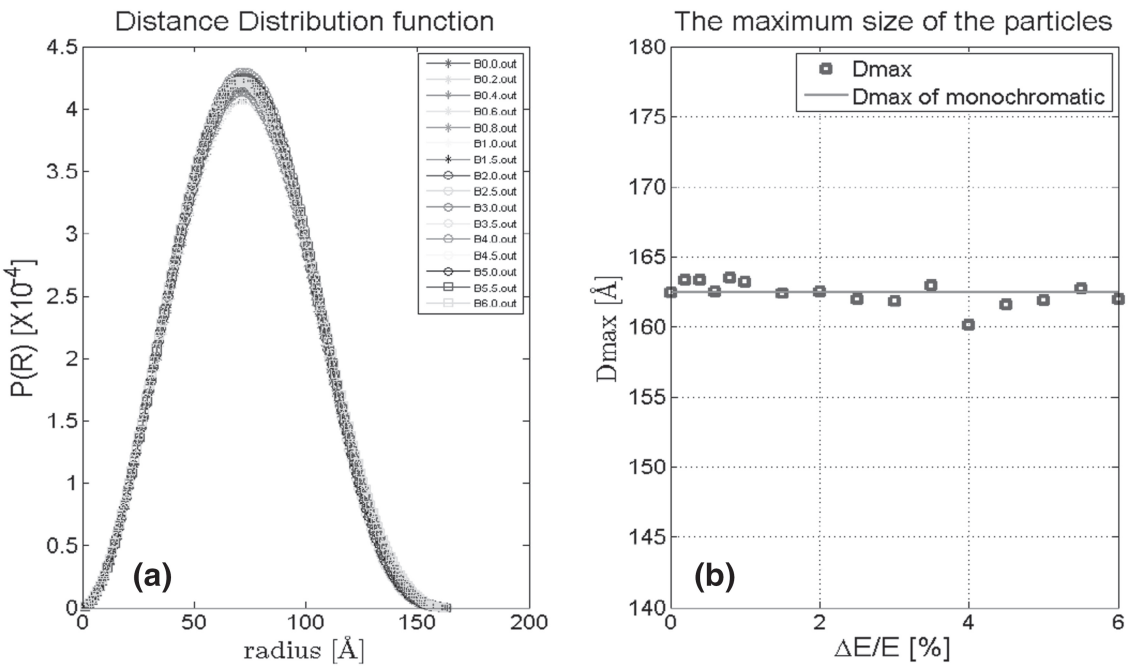

Fig. 6 **a** Distance distribution functions $P(r)$ for different energy bandwidths. **b** Maximum sizes of particles for different energy bandwidths (blue circles), and the maximum size of traditional monochromatic (red line) (color figure online)

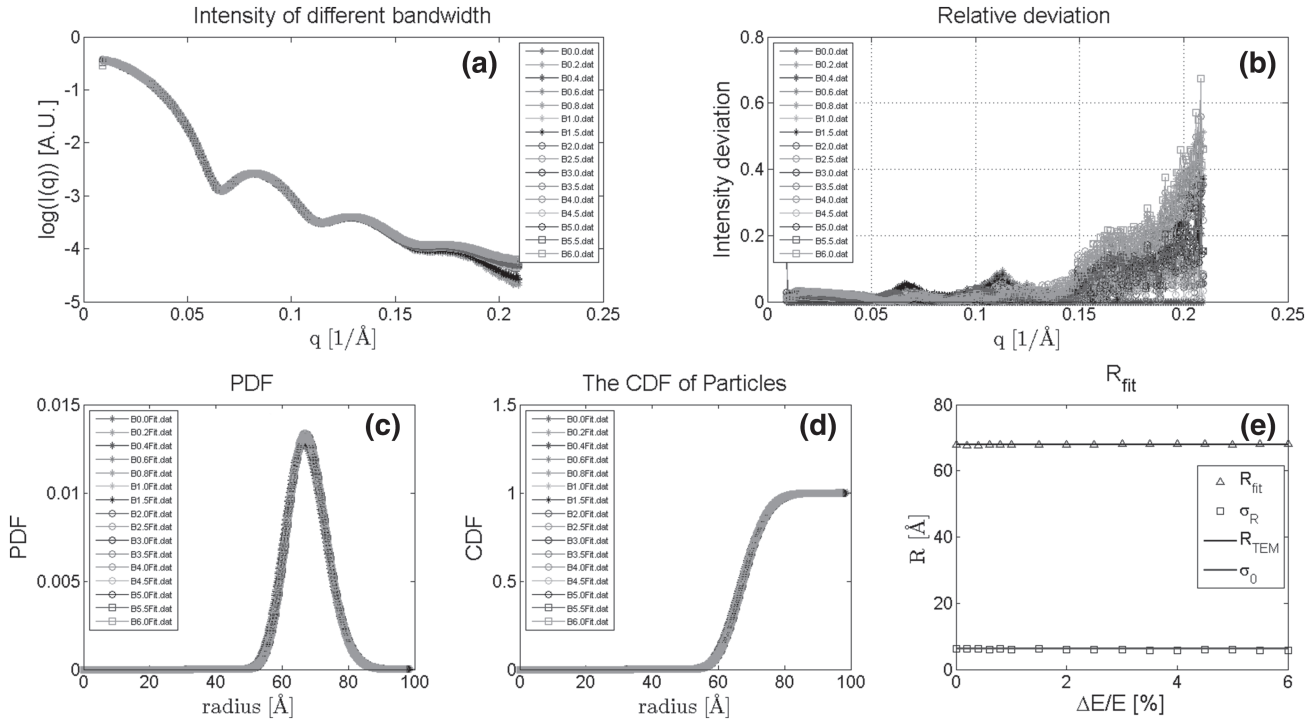

Fig. 7 **a** Normalized scattering curves. **b** The deviations of the pink beam from the traditional monochromatic beam. The PDF **c** and CDF **d** are obtained by SASfit for different energy bandwidths. **e** The mean sizes of the samples (red triangle) and the standard deviations (blue box) for different energy bandwidths. The black line is the mean size of samples measured by TEM, and the red line is the standard deviation for the traditional monochromatic beam (color figure online)

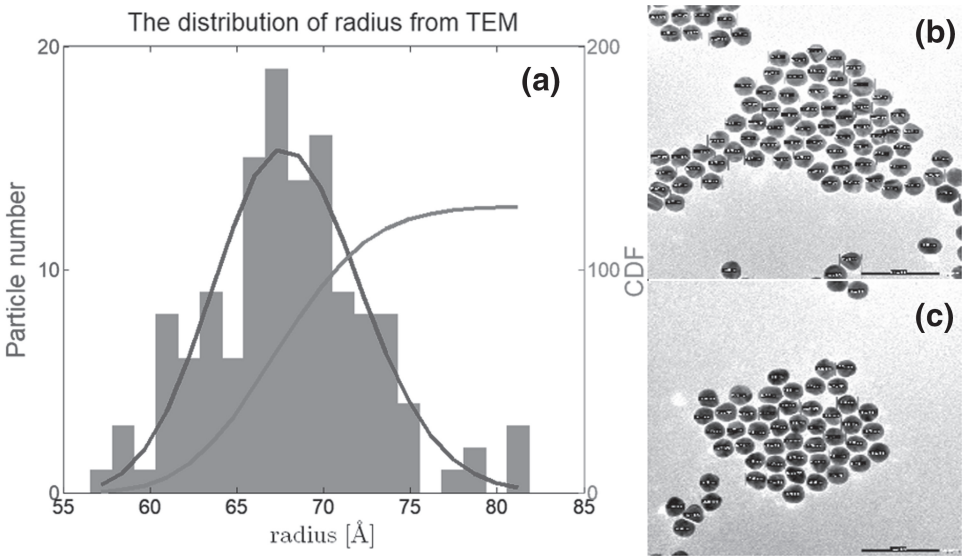

Fig. 8 TEM results of samples. The histograms in **a** are the particles number measured from TEM graphs shown in (**b**, **c**). The blue curve in **a** is the particles distribution density function fitted from the histograms which use a lognormal curve, and the green curve is the sums of histograms (color figure online)

$$f\,(R, N, \sigma, \mu) = \frac{N}{\sqrt{2\pi}\sigma R}\exp\left[-\frac{\ln\left(\frac{R}{\mu}\right)^2}{2\sigma^2}\right], \tag{3}$$

$$I\,(q, R, \Delta\eta) = \left\{\frac{4}{3}\pi R^3 \Delta\eta\left[3\frac{\sin(qR) - qR\cos(qR)}{(qR)^3}\right]\right\}^2, \tag{4}$$

where R is the radius of the spheres, $\Delta\eta$ the scattering length density difference between the particle and the matrix, σ the width parameter, μ the median radius of spheres and N the particle number density parameter. Using these parameters, the mean radius was calculated as $R_{\text{mean}} = \mu * \exp\left(\sigma^2/2\right)$ and the standard deviation of the width of the size distributions as $\sigma_{\text{width}} = \left[\mu^2\left(\exp\left(\sigma^2\right) - 1\right)\exp\left(\sigma^2\right)\right]^{1/2}$.

Equation (2) is employed for the interpretation of the scattering data by SASfit, and the results are shown in Fig. 7c–e. Curves in Fig. 7c, which represent the probability of particle size distribution (PDF), show that the PDFs for different bandwidths overlap with each other very well, even when the energy bandwidth increases to 6%. Mean radius and particle size distribution width are shown in Fig. 7e, and the deviations of mean radius are less than 0.5%. The mean radius and relative distribution width of the traditional monochromatic beam are $R_{\mathrm{mean}} = 67.9\,(1)$ Å and $\sigma_{\mathrm{width}}/R_{\mathrm{mean}} = 0.09\,(1)$, respectively.

Comparison with TEM

TEM measurements were taken to verify the results obtained by SAXS. The results of TEM are shown in Fig. 8. The particle size distribution was extracted from Fig. 8b, c, which is shown in the form of histogram in Fig. 8a. Fits of lognormal functions in PDF and CDF presentation are displayed as blue and green lines in Fig. 8a, respectively. The size information of more than 100 particles were obtained by TEM test, as shown in the green axis in the figure. The mean radius of the sample particles obtained by the lognormal function is $R_{\mathrm{mean}} = 67.8$ Å, and the relative distribution width is $\sigma_{\mathrm{width}}/R_{\mathrm{mean}} = 0.06$. Comparison of these TEM results with that of experiment reveals an excellent agreement of TEM and SAXS values. Therefore, it can be concluded that the TEM measurements confirm the results from SAXS.

Conclusion

The influence of the energy bandwidth on SAXS experiment has been studied through the simulation and the experiment. A SAXS system with an adjustable energy bandwidth was designed at beamline 1W2B, BSRF. The shape and size distribution, radius of gyration (Rg), the maximum size (Dmax) and the distance distribution function of the particles were analyzed with the pink beam. The results indicate that the structure information obtained from the pink beam and the traditional monochromatic beam is in accord with each other. In order to prove the feasibility of using smeared data for analyzing, the TEM test was also performed and consistent with that of the pink beam experiments. Through this work, we claimed that the signal acquired could be enhanced by increasing the energy bandwidth of the incident beam for weak signal samples and time-resolved SAXS experiments and the collected data could be directly analyzed using traditional methods.

Acknowledgements This work was supported by a grant from the National Key R&D Plan of China (Grant No. 2016YFA0401300).

References

1. P. Debye, A.M. Bueche, J. Appl. Phys. A **20**(6), 518 (1949)
2. G. Porod, *Small Angle X-ray Scattering* (Academic Press, London, 1982), pp. 17–51
3. J.S. Pedersen, Adv. Colloid Interface Sci. A **70**, 171 (1997)
4. D. Schneidman-Duhovny, S.J. Kim, A. Sali, BMC Struct. Biol. A **12**, 17 (2012)
5. Z.-H. Li, Chin. Phys. C A **37**(10), 108002 (2013)
6. S. Bratos et al., J. Synchrotron Radiat. A **21**(Pt 1), 177 (2014)
7. M. Rivers, Conference on Developments in X-Ray Tomography X. A, vol. 9967 (2016). https://doi.org/10.1117/12.2238240
8. O. Bilsel, C.R. Matthews, Curr. Opin. Struct. Biol. A **16**(1), 86 (2006)
9. M. Bagge-Hansen et al., J. Appl. Phys. A **117**(24), 245902 (2015)
10. R.L. Gustavsen et al., J. Appl. Phys. A **121**(10), 105902 (2017)
11. R. Takahashi, T. Narayanan, T. Sato, J. Phys. Chem. Lett. A **8**(4), 737 (2017)
12. T.M. Willey et al., AIP Conference Proceedings, vol. 1793 (2017), p. 030012. https://doi.org/10.1063/1.4971470
13. W. Wang et al., J. Appl. Crystallogr. A **48**(6), 1935 (2015)
14. B.R. Pauw, J. Phys. Condens. Matter. A **26**(23), 239501 (2014)
15. B.R. Pauw et al., J. Appl. Crystallogr. A **50**(6), 1800 (2017)
16. S. Chen, S.-N. Luo, J. Synchrotron Radiat. A **25**(2), 496–504 (2018)
17. E. Bergbäck Knudsen et al., J. Appl. Cryst. A **46**(3), 679 (2013)
18. D.I. Svergun, J. Appl. Cryst. A **25**, 495 (1992)
19. H.D. Mertens, D.I. Svergun, J. Struct. Biol. A **172**(1), 128 (2010)
20. O. Glatter, R. Klein, P. Lindner, *Neutrons, X-ray and Light: Scattering Methods Applied to Soft Condensed Matter*, 1st edn. (Elsevier, Amsterdam, 2002), pp. 391–420
21. A. Guinier, G. Fournet, *Small Angle Scattering of X-Rays* (Wiley, New York, 1955)
22. K. O'grady, A. Bradbury, J. Megn. Megn. Mater. A **39**, 91 (1983)
23. M. Bonini, E. Fratini, P. Baglioni, Mater. Sci. Eng. C A **27**(5–8), 1377 (2007)
24. B.R. Pauw, C. Kastner, A.F. Thunemann, J. Appl. Crystallogr. A **50**(Pt 5), 1280 (2017)
25. S.M. Sedlak, L.K. Bruetzel, J. Lipfert, J. Appl. Crystallogr. A **50**(Pt 2), 621 (2017)
26. J.S. Pedersen, D. Posselt, K. Mortensen, J. Appl. Crystallogr. A **23**, 321 (1990)
27. P.V. Konarev et al., J. Appl. Crystallogr. A **36**, 1277 (2003)
28. W. Szczerba et al., J. Appl. Crystallogr. A **50**(Pt 2), 481 (2017)